Marine and Petroleum Geology 133 (2021) 105302

Contents lists available at ScienceDirect

Marine and Petroleum Geology

journal homepage: www.elsevier.com/locate/marpetgeo

# Seismic imaging of an active fluid conduit below Scanner Pockmark, Central North Sea

Bettina Schramm [a,*], Christian Berndt [a], Anke Dannowski [a], Christoph Böttner [b], Jens Karstens [a], Judith Elger [a]

[a] GEOMAR Helmholtz Centre for Ocean Research Kiel, Wischhofstraße 1-3, Kiel, Germany
[b] Christian-Albrechts-Universität zu Kiel, Institute of Geosciences, Christian-Albrechts-Platz 4, Kiel, Germany

ARTICLE INFO

*Keywords:*
P wave velocity
3D travel-time tomography
Fluid flow
Scanner pockmark
Ocean-bottom seismometer
Wide-angle seismic

ABSTRACT

Subsurface $CO_2$ storage is a key strategy to reduce greenhouse gas emission, but leakage of $CO_2$ along natural fluid pathways may affect storage formation integrity. However, the internal structure and the physical properties of these focused fluid conduits are poorly understood. Here, we present a three-dimensional seismic velocity model of an active fluid conduit beneath the Scanner Pockmark in the Central North Sea, derived from ocean-bottom seismometer data. We show that the conduit, which manifests as a pipe structure in seismic data, is separated into two parts. The upper part, extending to 260 m depth, i.e. 110 m below the seafloor, is characterised by seismic velocities up to 100 m/s slower than the surrounding strata. The deeper part is characterized by a 50 m/s seismic velocity increase compared to background velocity. We suggest that the upper part of the pipe structure represents a network of open fractures, partly filled with free gas, while the reason for the velocity increase in the lower part remains speculative. These observations suggest that active pipes can be internally heterogeneous with some intervals probably being open fluid pathways and other intervals being closed. This study highlights the complexity in evaluating focused fluid conduits and the necessity of their detailed assessment when selecting $CO_2$ storage sites.

## 1. Introduction

The increasing concentration of greenhouse gases in the atmosphere is one of the major challenges of the 21st century. The Intergovernmental Panel on Climate Change (IPCC) identified carbon dioxide capture and storage (CCS) as a key component of mitigation strategies to reduce $CO_2$ concentration in the atmosphere in order to limit global warming to 1.5 °C by the end of this century (IPCC, 2018). Saline aquifers and depleted hydrocarbon reservoirs in the North Sea Basin are the most promising storage formations for the industrial-scale implementation of CCS in Europe (Haszeldine, 2009).

In the North Sea, natural fluid migration structures are commonplace, and manifest in seismic reflection data as pipes and chimneys (Karstens and Berndt, 2015). Pipes and chimneys are the seismic expression of vertical, strata-cutting, focused fluid conduits with chaotic seismic facies and reflections with increased or reduced seismic amplitude (Moss and Cartwright, 2010; Løseth et al., 2011; Andresen, 2012; Cartwright and Santamaria, 2015; Karstens and Berndt, 2015). Both are columnar and can reach from a few tens of meters in diameter to more than 2 km in diameter. We follow the Karstens et al. (2019) nomenclature of calling pipes those structures that are comparably narrow and have sharp vertical boundaries while calling chimneys those with an irregular boundary to the host rock, but we acknowledge that there are different usages of these terms in the literature. Based on the multi-channel seismic (MCS) data presented in this study and the results of Böttner et al. (2019), we will label the focused fluid conduit beneath the Scanner Pockmark as a pipe structure in the following.

Generally, the formation of these pathways is believed to be controlled by overpressure-induced hydrofracturing of an impermeable cap rock (Hubbert and Willis, 1957; Clayton and Hay, 1994; Cathles et al., 2010). However, it is unclear how long these structures remain open for fluid migration after their formation (Karstens and Berndt, 2015). Pipes and chimneys may represent a direct connection from deep reservoirs to the seafloor and feed active seafloor seeps (Hovland and

* Corresponding author.
*E-mail addresses:* bschramm@geomar.de (B. Schramm), cberndt@geomar.de (C. Berndt), adannowski@geomar.de (A. Dannowski), christoph.boettner@ifg.uni-kiel.de (C. Böttner), jkarstens@geomar.de (J. Karstens), jelger@geomar.de (J. Elger).

https://doi.org/10.1016/j.marpetgeo.2021.105302
Received 15 April 2021; Received in revised form 18 August 2021; Accepted 19 August 2021
Available online 21 August 2021

Sommerville, 1985; Schneider von Deimling et al., 2007; Løseth et al., 2011). The internal structure and the physical properties of pipe and chimney structures are poorly understood as they are generally avoided during drilling operations and have rarely been the subject of detailed geophysical studies. Notable exceptions are chimney structures above the Tommeliten Alpha Field (North Sea), where seismic shear wave experiments, numerical simulations and wellbore data revealed a gas-filled fracture network (Granli et al., 1999; Arntsen et al., 2007) and in the Nyegga Region (Norwegian Sea), where the abundance of gas hydrates in the conduit was studied using seismic tomography (Plaza--Faverola et al., 2010).

Seismic reflection profiling is a powerful tool to identify vertical heterogeneities such as pipe structures. However, conventional reflection seismic surveys have significant shortcomings in imaging the internal structure of focused fluid conduits, in differentiating between real geological structures and imaging artefacts in such settings (Løseth et al., 2011; Karstens and Berndt, 2015), and they cannot be used to reconstruct their hydraulic properties. Seismic velocity models may provide valuable information about the internal structure of focused fluid conduits. They can provide information on the type of pore fill, e.g. gas or aqueous fluids, and qualitative information on porosity as it correlates with seismic velocity. Seismic anisotropy and lateral velocity changes that correlate with seismic reflection patterns may also constrain the hydraulic permeability. To derive high-resolution seismic velocity models, we have conducted a three-dimensional (3D) ocean-bottom seismometer (OBS) experiment. The survey layout provided for shots from all directions and long offsets between the shots and the recording instruments. Overall, the data have a good signal-noise ratio.

Seismic forward modelling of OBS data allows to construct detailed velocity models (Zelt, 1998; Plaza-Faverola et al., 2010) as long as the data are sampled densely enough to resolve the velocity variations in the subsurface. Previous studies have mainly used sparse data along 2D seismic lines resulting in rather sparse and undersampled models that may easily be affected by erroneous assignment of arrivals because of side reflections. In this study, we use a very densely sampled 3D OBS data set covering a wide range of offsets and azimuths to derive seismic velocity anomalies within and around the fluid conduit beneath the Scanner Pockmark (Fig. 1). The objective is to put these derived velocity anomalies into context with other geological and geophysical information to elucidate the functioning of fluid pathways. Furthermore, we investigate the role of free gas in the formation of pipe structures and constrain the source of ascending fluids beneath the Scanner Pockmark.

## 2. Geological setting

The Scanner Pockmark Field is located within the Witch Ground Graben (Fig. 2), which developed from the Triassic to the early Cretaceous as part of the North Sea Basin failed rift system (Judd et al., 1994; Glennie, 1998). The basin was a major centre of deposition during the late Jurassic and in the early Cretaceous, as well as during the Quaternary (Judd et al., 1994). Clays with interbedded sandstones and limestones dominate the Paleogene and Neogene sequences. The shallow sediments of the Early Pleistocene Aberdeen Ground Formation show evidence for subglacial, glaciomarine and marine deposition (Sejrup et al., 1987; Reinardy et al., 2017; Rea et al., 2018). The top of the Aberdeen Ground Formation is a regional glacial unconformity, which corresponds to the advance of grounded ice sheets into the North Sea Basin during the Mid-Pleistocene (Fig. 2; Reinardy et al., 2017). Many tunnel valleys incise into the Aberdeen Ground Formation and into the overlying Ling Bank Formation, representing different phases of glacial erosion and deposition with poorly constrained ages. The upper Mid to Late Pleistocene sediments consist of the Coal Pit, Swatchway and Witch Ground Formations (Fig. 2; Böttner et al., 2019). The Coal Pit Formation consists of glacial tills with hard dark grey to brownish-grey, muddy, pebbly sands or sandy muds deposited between Marine Isotope Stage (MIS) 3 and 6 (Andrews et al., 1990; Graham et al., 2010; Stoker et al., 2011). The Swatchway Formation comprises silty to sandy clays with rare pebbles; these possibly proximal glaciomarine sediments were deposited during MIS 2 and 3. The Witch Ground Formation consists of finely laminated glaciomarine sediments, which were deposited during MIS 1 and 2 (Fig. 2; Stoker et al., 2011).

The entire North Sea Basin is affected by focused flow of hydrocarbons from deep thermogenic sources, strongly mixed with microbially-formed shallow methane (Karstens and Berndt, 2015; Chand et al., 2017). Two types of pockmarks occur in the study area (Hovland et al., 2010; Böttner et al., 2019): smaller pockmarks (0.9–3.1 m deep, 26–140

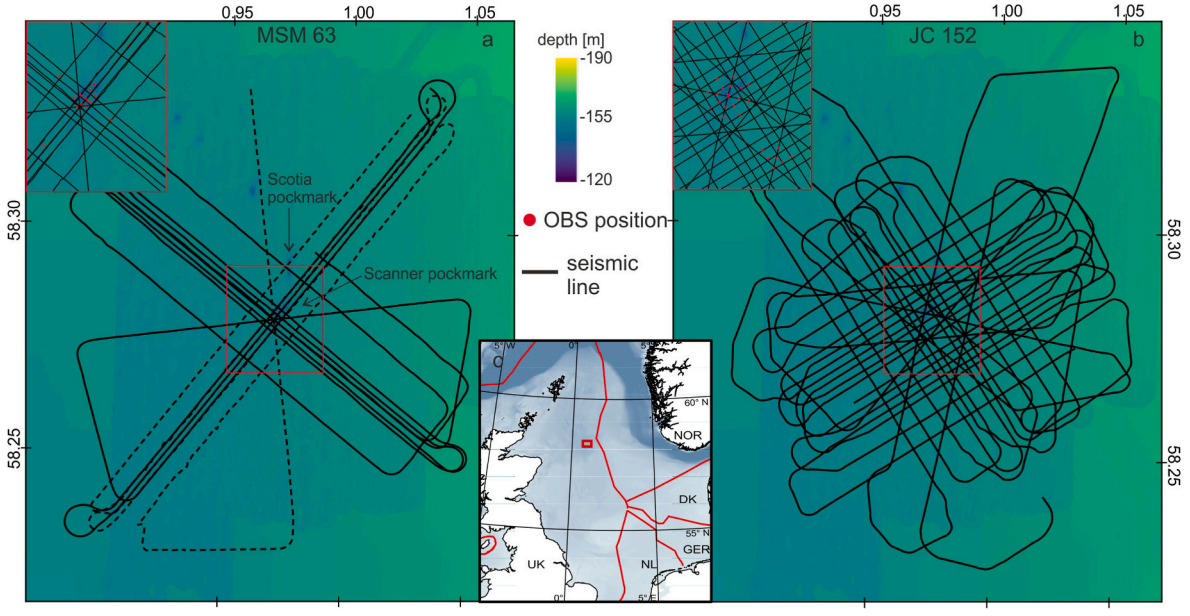


**Fig. 1.** Location of the Scanner Pockmark. Map of the seismic experiment and the bathymetry of the Scanner Pockmark, showing the seismic lines (P1000: dashed line; P2000: line drawn through) and the OBS deployment sites (red dots) of research cruises a) MSM 63 and b) JC152. c) Location of the study area block 15/25b in the Central North Sea. The bathymetric data were acquired during this study, while gaps and the surrounding area were filled with bathymetric data from Emodnet-Bathymetry (Schapp and Schmitt, 2017). (For interpretation of the references to colour in this figure legend, the reader is referred to the Web version of this article.)

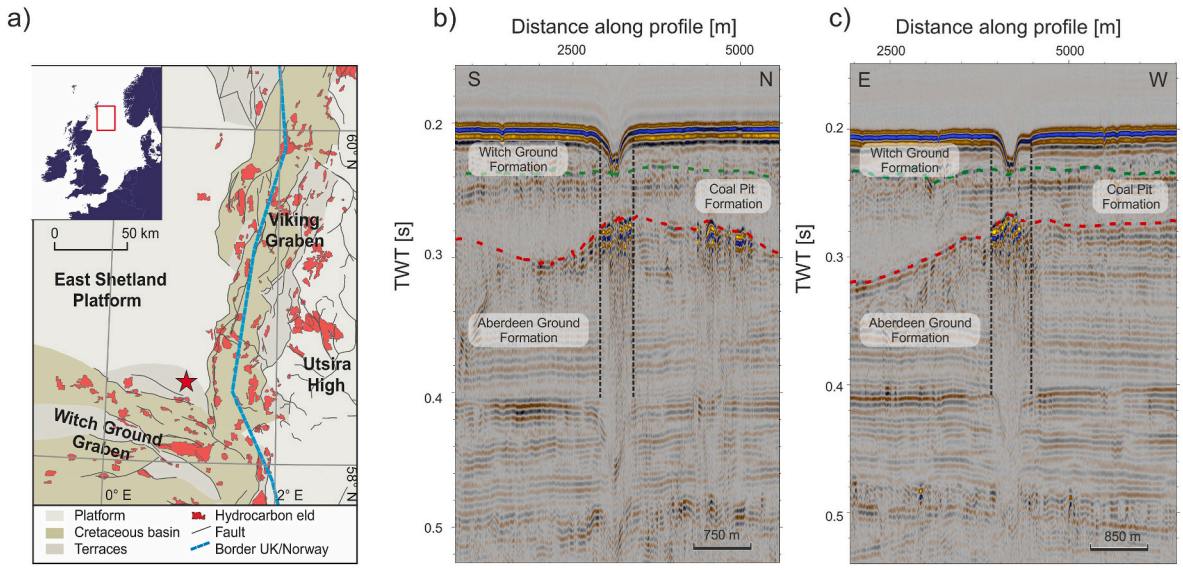


**Fig. 2.** Geological setting. a) Geological map of the Central North Sea with the location of the study area (red star). Seismic sections across the Scanner Pockmark b) in South-North and c) East-West direction with the main stratigraphic units. (For interpretation of the references to colour in this figure legend, the reader is referred to the Web version of this article.)

m long, and 14–57 m wide) that only affect the post-glacial successions, and unusually large pockmarks (>6 m deep, >250 m long, and >75 m wide). The Scanner and Scotia pockmarks (Fig. 1) are unusually large examples of this second class (Judd et al., 1994; Gafeira and Long, 2015, Böttner et al., 2019). Exploration-type 3D reflection seismic data show almost circular seismic amplitude anomalies below the pockmarks down to a depth of several hundred meters (Böttner et al., 2019). These anomalies do not match the distribution of free gas in the shallow

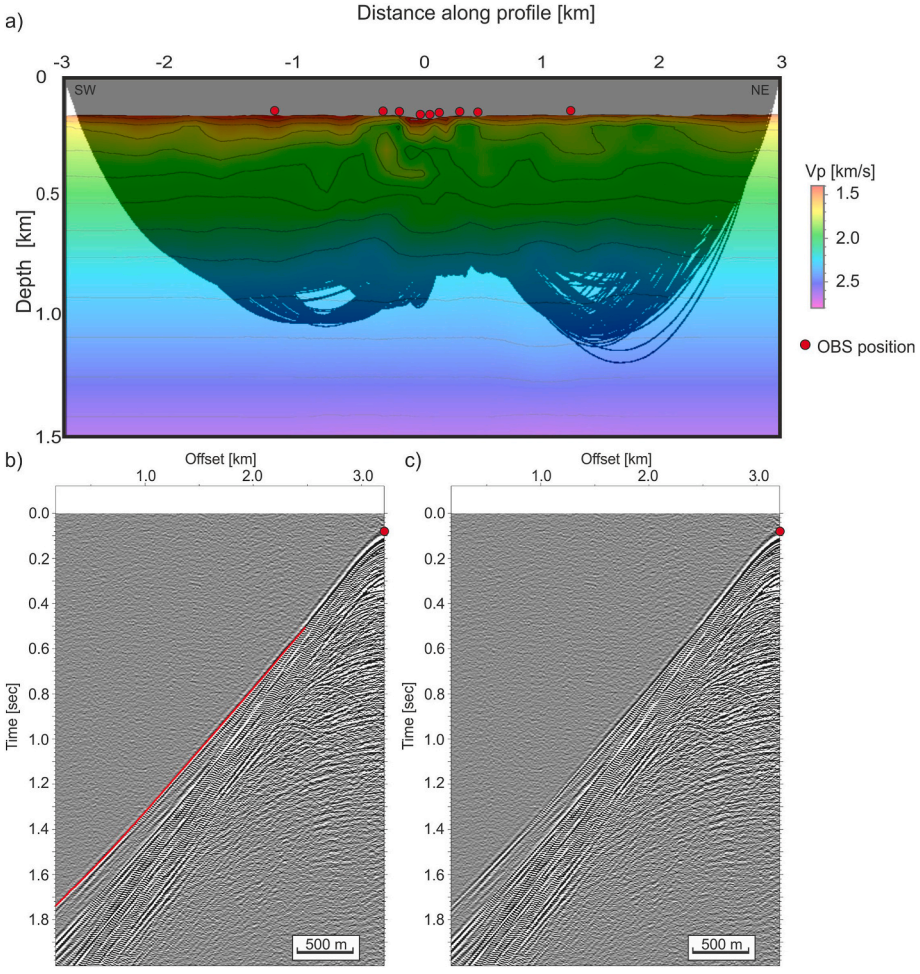


**Fig. 3.** Data example. a) Velocity distribution along a SW-NE profile crossing the Scanner Pockmark. The displayed ray paths (black lines) show the zone were the velocity model is well constrained. The red circles mark the OBS positions. b) Seismic section recorded by OBS with the interpreted refractions (red line) used for modelling with FAST and c) without the interpreted refractions. (For interpretation of the references to colour in this figure legend, the reader is referred to the Web version of this article.)

subsurface suggesting that they are not seismic artefacts but caused by real geological structures (Fig. 2). Persistently observed acoustic anomalies in the water column inside and above the pockmark have be interpreted suggest that the pockmarks continuously release deeply-sourced methane that is advected through the pipe structures (Böttner et al., 2019).

## 3. Data

We used three different data sets: newly acquired high-resolution 3D OBS and 2D MCS data, and an industry 3D MCS dataset ("CNS MegaSurveyPlus") provided by PGS, Oslo. During research cruise MSM63 in April/May 2017 on board R/V Maria S. Merian, 15 OBSs were deployed around and inside the Scanner Pockmark. The spacing of the OBSs varied between 100 m and 1000 m in water depths between 150 and 170 m (Fig. 1). A GI-gun array consisting of two 210-inch$^3$-GI-guns (G = 105 in$^3$/I = 105 in$^3$) served as the seismic source. The pressure was kept at 210 bar and the array was towed at 2 m water depth, which provided a frequency band of 15–500 Hz. The shot interval was 10 s (survey P1000). The OBSs recorded continuously for 9 day at a sampling rate of 500 Hz. In general, the data quality was excellent (Fig. 3). Processing of these data included a minimum phase Ormsby band-pass-filter (15-20-200-300 Hz). Due to strong currents, instruments drifted away from their dropping position, on average 30 m. The largest drift was 70 m. The relocation procedure minimized the least square misfit between the observed direct wave arrival and the synthetic arrival calculated based on the bathymetric data collected during the MSM63 survey. For the relocation we used the average velocity of the water column, 1.48 km/s, which was measured by a sound velocity profile at the beginning and at the end of the cruise. The quality of the 3D tomography depends on accurate OBS locations. In this study we were able to obtain an accuracy of about 1 m.

The OBS data were complemented by 2D MCS data (survey P2000) that were recorded during the same research cruise (Fig. 1a). For the acquisition of the 2D reflection seismic data we used a 150 m-long streamer consisting of 96 channels with a 1.5625 m group spacing. We used the same seismic source and pressure, but the shot interval was reduced to 5 s. Processing of the MCS data included geometry and delay corrections, static corrections, common mid-point binning to 1.5625 m and bandpass filtering with corner frequencies of 25, 45, 420, and 500 Hz. A normal move-out correction with a constant velocity of 1.48 km/s (measured by a water sound velocity probe) was applied and the data were stacked and then migrated using a 2D Stolt algorithm. To compare the reflection seismic image with the velocity model derived from tomographic inversion of the OBS data, we have converted the 2D seismic data from two-way travel time to depth using a single velocity depth function (Table 1). This conversion does not account for lateral velocity variations, but as these velocity variations and layer thickness variations are small, the assumption of a simple velocity field results in a vertical error of less than 10 m at a depth of 300 m. This mismatch is far below the 50 m forward node interval for the tomographic inversion and hence accurate enough for the comparison.

During the same summer season, a second OBS dataset was acquired during RRS James Cook cruise JC152. An array of 25 OBSs was deployed within and around the pockmark and on a reference site southeast of the Scanner Pockmark (Fig. 1b). The source also consisted of a GI-Gun array of two 210-inch$^3$-GI-guns (G = 105in$^3$/I = 105 in$^3$). It was towed at 2 m water depth behind the vessel with the same configuration as that during MSM63. The shot interval was 8 s and the data were recorded at a sampling rate of 4000 Hz.

The 3D industry seismic data covers more than 22,000 km$^2$ of the central northern North Sea, including the Scanner Pockmark, down to 1.5 s two-way travel time (TWT). This 3D pre-stack time-migrated dataset has a vertical resolution of approximately 20 m with an inline and crossline spacing of 12.5 m (see Böttner et al., 2019).

**Table 1**
Single velocity depth function for converting the 2D seismic data to depth.

| MCS (depth [m]) | MCS (TWT [s]) | Interval Velocity (m/s) |
|---|---|---|
| 0 | 0 | |
| 149 | 0.2 | 1490 |
| 300 | 0.37 | 1798 |
| 500 | 0.56 | 2073 |
| 1000 | 1 | 2299 |
| 2000 | 1.630 | 3155 |

## 4. 3D seismic traveltime tomography

First-arrival time tomography aims to reconstruct the P-wave velocities of the Earth's interior. First-arrival times of seismic shots calculated through an initial model are compared to the observed travel times, based on the shortest ray path. The initial model is modified until the best possible fit between model predictions and observed data is found.

To build a detailed 3D seismic velocity model based on the collected OBS data, we used FAST (First Arrival Seismic Tomography), a 2D and 3D first arrival travel time tomography package, including forward modelling and inversion (Zelt and Barton, 1998). The 3D model space is 1.5 km deep and covers an area with a lateral extent of 6 km × 6 km with the Scanner Pockmark at the centre. The grid node spacing for the forward modelling is 10 m in all directions. The grid cell size of the inversion is 100 m in x and y direction and 100 m in depth. Our starting model consists of two layers: the first layer is the water column and has a constant seismic velocity of 1.48 km/s based on sound velocity probe measurements. The seafloor interface and the water velocity were kept fixed during tomographic inversion for the seismic velocities within the subsurface. As FAST is influenced by the initial model it was important to check for the influence of the choice of the second layer, i.e. from the seafloor to the base of the model domain, velocity on the inversion result. Therefore, we tested 100 initial models in which we introduced up to ± 100 m/s seismic velocity anomalies on a regional North Sea background model (Fig. 4). We analyzed the inversion results and chose a starting model (in the following called the preferred model) that is characterized by small $\chi^2$ values and which is producing similar anomalies to the majority of other starting models. In the following we only discuss seismic velocity anomalies that are produced after 10 iterations and that are independent on the starting model.

We picked the seismic first arrivals with the seismic interpretation software IHS Kingdom Suite. Errors resulting from automatic picking were corrected manually. Reflections below the seafloor were difficult to identify due to superposition with multiples below ~300 ms TWT, the effects of blanking inside the pipe, and the ghost signal from the airgun. We assigned the picks an uncertainty of 8 ms. This yielded a $\chi^2$ of 1.0029 and a root-mean-square (RMS) misfit of 8.0115 ms in the best-fitting model, which converged within 10 iterations (initial RMS misfit of 19 ms). The misfits are consistent for the different instruments. Overall, our dataset contains more than 180,000 P-wave first arrival picks with a maximum offset of 3 km.

In order to avoid misinterpretation of structures appearing in the travel time tomography, the lateral resolution of the velocity must be known (Zelt, 1998). Our study region is strongly affected by focused flow of hydrocarbons from deep thermogenic sources, mixed with microbially formed shallow methane, which cause seismic velocity anomalies (Karstens and Berndt, 2015; Chand et al., 2017). To determine the limits of lateral resolution we have conducted a checkerboard test (Fig. 5) and several characteristic tests (Fig. 6) (Zelt, 1998; Leveque et al., 1993; Schmelzbach et al., 2008). The checkerboard test was run with a checkerboard pattern of 0.5 × 0.5 × 0.5 km size and 20% of velocity anomalies compared to the preferred model. The results of the checkerboard test show that our tomographic setup allows the recovery of the injected anomalies below the Scanner pockmark and up to a depth

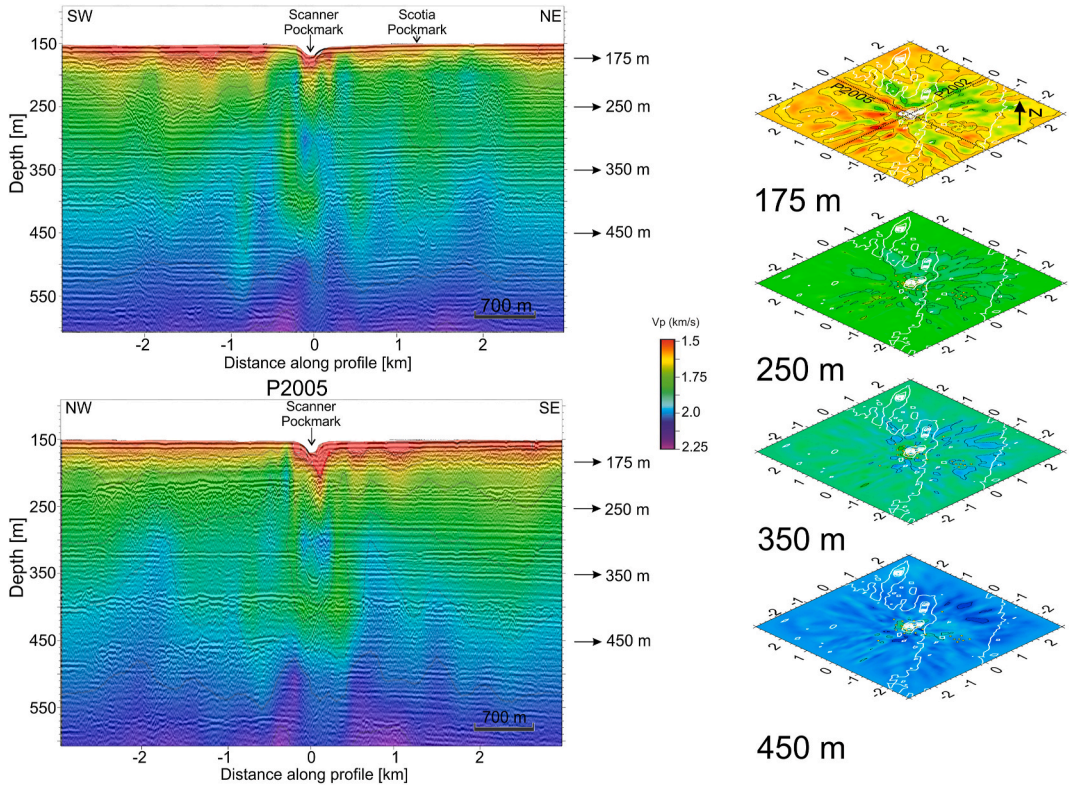


**Fig. 4.** Average of 100 inversion runs of the seismic tomography with a random created initial model. Velocity distribution a) in SW-NE direction and b) in NW-SE direction. Each section shows a clear negative seismic velocity anomaly beneath the Scanner pockmark. c) Depth slices of the seismic velocity field for 175 m, 250 m, 350 m and 450 m depth. The white isolines image the seafloor topography.

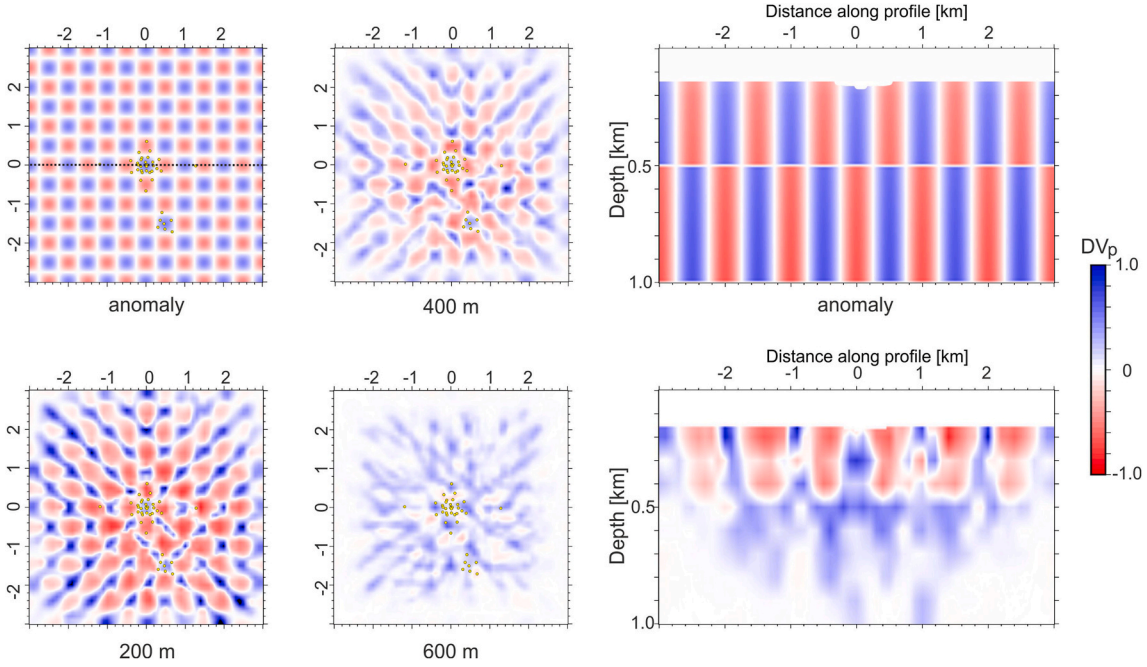


**Fig. 5.** Checkerboard test with a synthetic anomaly of 0.5 × 0.5 × 0.5 km in size and a velocity perturbation of 20%. The yellow dots mark the OBS locations. (For interpretation of the references to colour in this figure legend, the reader is referred to the Web version of this article.)

of 500 m (Fig. 5). Satisfactory inversion statistics ($\chi^2 = 1.8658$ and RMS = 12.86795 ms) were obtained at the end of the 5th iterations. All first-arrival tomographies have a lambda of 50 (Zelt, 1998).

In addition to the checkerboard test, we carried out several characteristic tests. Characteristic tests contain anomalies of similar amplitude as the real one but with different sizes and shapes (Haslinger et al., 1999; Husen et al., 2000). For these tests we introduced single velocity anomalies with a velocity decrease of 20% directly starting beneath the Scanner Pockmark and reaching down to 300, 500, and 1000 m and one with a 20% decreased seismic velocity in the top 300 m and a 20%

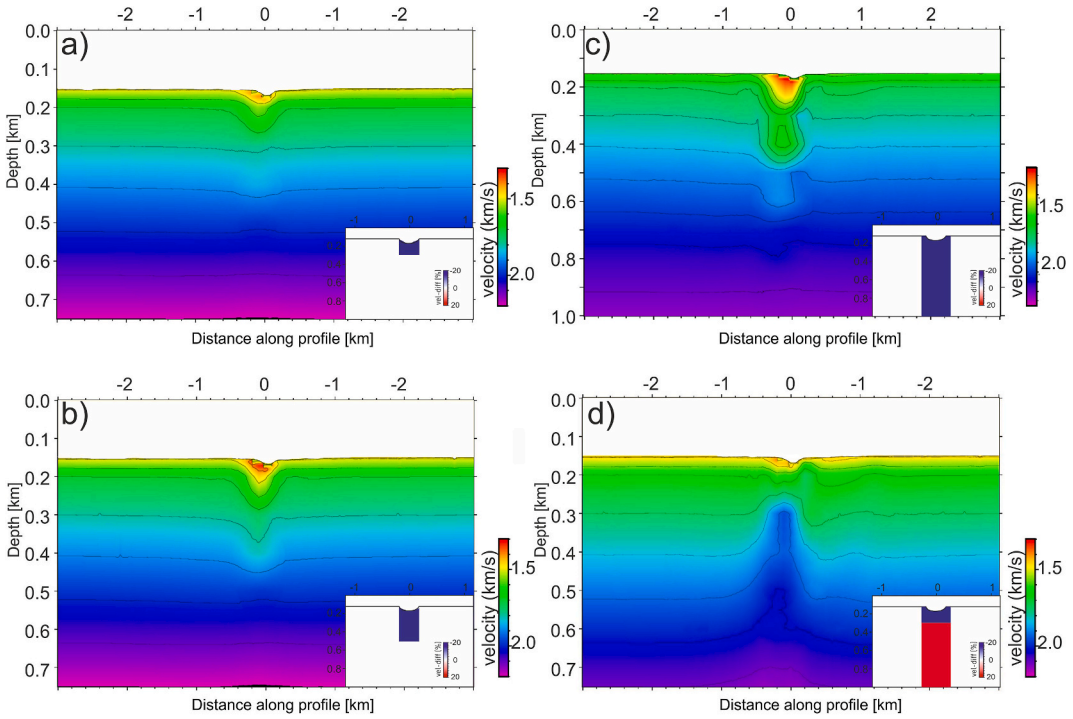


**Fig. 6.** Characteristic test with different initial models beneath the Scanner Pockmark. The injected anomaly (insets) is a velocity difference of −20% compared to the initial model of our preferred model. The injected negative anomalies extend to depths of a) 300 m, b) 500 m, c) 1000 m and d) 300 m with a positive anomaly below.

velocity increase from 300 to 1000 m depth. For these models the rays were calculated by ray tracing and used for tomographic inversion. We analyzed the results after 10 iterations. The velocity model for the characteristic tests is based on the width and shape of the seismic anomaly below Scanner Pockmark as observed in the 3D reflection seismic data (Böttner et al., 2019) and has a velocity anomaly which is circular and has a diameter of 200 m. Again, the background model is based on our preferred model. The characteristic tests show that a

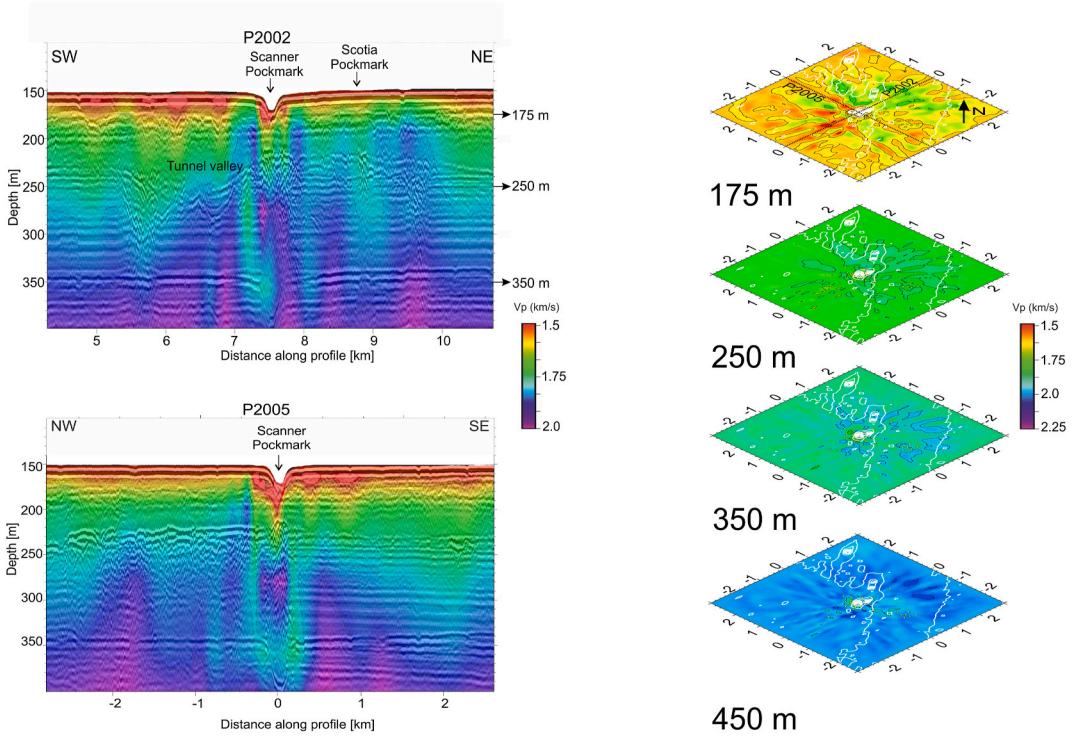


**Fig. 7.** Velocity distribution. a) in SW-NE direction and b) in NW-SE direction. Each section shows a clear negative seismic velocity anomaly beneath the Scanner pockmark. c) Depth slices of the seismic velocity field for 175 m, 250 m, 350 m and 450 m depth. The white isolines image the seafloor topography, one isoline is every 2 m.

velocity anomaly beneath the Scanner pockmark can be well resolved by our tomographic setup down to 750 m depth. With greater depth the resolution decreases. These smearing effects are typical for strong lateral velocity variation, when smoothing is applied during the inversion. In addition, the characteristic tests show that no low velocity zones are created as a result of the tomographic inversion. Thus, the inverted velocities allow us to differentiate between pipe segments with decreased seismic velocities that may reflect increased gas content or disrupted sediments and pipe segments with increased seismic velocities, e.g. due to cementation or different lithologies.

## 5. Results

### 5.1. P-wave velocity model from FAST

The results of the first arrival travel time tomography show considerable lateral velocity variations in the area beneath the Scanner Pockmark and the surrounding area. The region beneath the pockmark is characterized by a decrease in seismic P-wave velocity (Vp) inside the pipe structure compared to the area surrounding it (Fig. 7). From the seafloor down to 260 m depth (in the following all depth values refer to depth below sea level), the velocity inside of the pipe is up to 10% lower than in the surrounding background. For example, at 200 m depth the velocity drops from 1.7 km/s outside the pipe structure to 1.55 km/s inside. The velocity decrease coincides with a high-amplitude seismic anomaly in the 2D and 3D MCS data and the velocity anomaly is approximately 370 m wide in all directions. The location, the width and the magnitude of the velocity anomaly are robust for all starting models, i.e. it is reproduced by the inversion regardless of the chosen starting model and for different subsets of data. Below the Upper Aberdeen Ground Formation, the negative velocity anomaly beneath the Scanner Pockmark turns into a positive velocity anomaly that stretches from about 280 m depth to about 500 m below the sea surface (Fig. 7c). It is robust in the sense that it is produced by inversion of most starting models. The shape of the anomaly is nearly circular and becomes wider with greater depth, while the velocity difference is up to 0.05 km/s. The deeper part of the pipe structure, which is characterized by a positive seismic velocity anomaly, is surrounded by an area of lower seismic velocities (Fig. 7b).

Below 260 m depth, the inverted models for all starting models consistently show a velocity drop of about 0.1 km/s for the pipe structure compared to the surrounding formation. These low velocities occur approximately 500 m NW and the SE of the pipe (Fig. 7b).

Average velocities of 1.7–1.8 km/s characterize the tunnel valley in the Southwest of Scanner Pockmark. Only the most deeply incised part of the tunnel valley further in the SW is associated with velocities of 1.8–1.85 km/s. Seismic velocity decreases laterally to 1.8 km/s at 300 m next to the Scotia pockmark to the NE of the Scanner Pockmark (Fig. 7a).

Overall, the results of the travel time tomography show significant seismic velocity variations but the limited extent of the model is insufficient to determine a general background seismic velocity for the Quaternary sediments. Small-scale seismic velocity anomalies are ambiguous, but the low velocity anomalies below Scanner Pockmark and Scotia Pockmark are robust, including the high velocity anomaly below the Scanner Pockmark from 280 m to ~500 m depth and the surrounding, about 400 m-wide zones of slightly reduced velocities (Fig. 8a). Possibly the offset of the anomaly below Scotia Pockmark is a result of the survey layout with fewer ray paths sampling the subsurface in this region.

### 5.2. Correlation between MCS and tomography

To quantify the dimensions of the pipe structure beneath the Scanner Pockmark, we compare the 2D MCS data with the results of the travel time tomography. Beneath the pockmark, the MCS data show amplitude anomalies with zones of dimmed reflections and bright spots at different depth levels, e.g. at 280 ms and 350 ms TWT. The MCS data show increased seismic amplitudes at the lowest glacial incision surface below the Scanner and Scotia pockmarks and along the northern rim of the tunnel valley. In some places (Fig. 8c), these high-amplitude reflectors have reversed polarity with respect to the seafloor reflection (i.e. reflector at 280 ms TWT depth and 7000 m along the profile). The anomalies are limited to an interval of 20–30 ms TWT and they are commonly underlain by chaotic seismic facies. We used the seismic

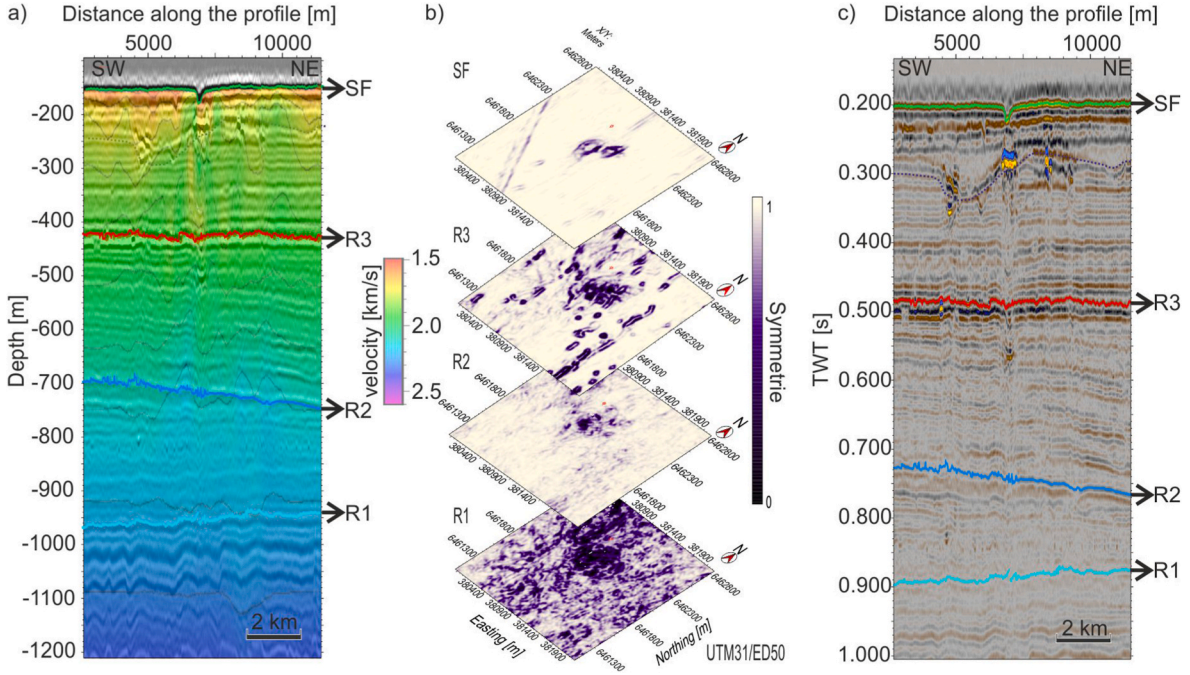


**Fig. 8.** Seismic section at the Scanner Pockmark. a) MCS data on which the Vp model has been overlain (profile P2002). b) 3D seismic attribute analysis based on conventional 3D seismic data. The similarity attribute is displayed for four stratigraphic horizons. c) MCS data (profile P2002) with respective seismic horizons with seismic stratigraphy from Böttner et al. (2019).

similarity attribute derived from the 3D seismic amplitude data to identify the spatial extent of these amplitude anomalies and their subsurface expression (Fig. 8b). The symmetry attribute is a post-stack, post-migration structural feature detection tool based on a 3D log-Gabor filter array (Yu et al., 2015) provided by the IHS Kingdom software. The horizon slices through the similarity volume show the pipe structure as an almost circular amplitude anomaly with a constant diameter at different depth levels. The comparison of the lateral extent of the pipe structure in the two data sets reveals a consistent discrepancy: the area of high amplitudes in the 3D MCS data is 280 m wide in diameter compared to a width of the velocity anomaly in the OBS tomography models of about 370 m (compare Figs. 7c and 8b).

The 3D MSC seismic data provide important insights into the regional geological setting. High amplitude patches (bright spots) with polarity reversals occur at most stratigraphic highs between the adjacent tunnel valleys that incise the Ling Bank Formation. These anomalies correspond to the low velocities in the tomographic models. A detailed seismic stratigraphic analysis (Böttner et al., 2019) showed that the seismic amplitude anomalies are the seismic expression of shallow free gas accumulations. The 3D seismic data also provide more details on the lateral variation of the tunnel valleys. The deeply incised tunnel valley SW of the Scanner Pockmark is a major structure that can be traced for several tens of kilometres. However, the vicinity of Scanner is different compared to the rest of the tunnel valley as it broadens from about 500 m to about 2500 m with a terrace close to Scanner Pockmark and a deeply incised part only at the SW edge of the tunnel valley (Fig. 8).

## 6. Discussion

### 6.1. Seismic artefact or geological feature

Seismic interpretation of fluid flow structures, especially when they are vertically orientated, can be ambiguous (Kristensen and Huuse, 2012; Karstens and Berndt, 2015). Further analysis of the pipe structure interpreted underneath the Scanner Pockmark thus requires an assessment to what extent the geophysical observations support the presence of a real geological structure and to what extent the observations are the result of imperfect geophysical imaging. Often, effects like blanking beneath gas accumulations, migration artefacts due to insufficiently resolved lateral velocity variations at shallow depth or bad seismic traces may lead to misinterpretation as seismic pipes (Karstens and Berndt, 2015). Böttner et al. (2019) conclude in their discussion about the limitations of 3D seismic imaging that a geological structure at Scanner exists because the anomaly in the seismic data does not coincide spatially with the seismic evidence of free gas in the subsurface. Furthermore, the structure is associated with distinct seismic observations such as downlaps that cannot be explained by seismic wave propagation artefacts. Our seismic tomography results show a distinct and starting-model-independent seismic velocity anomaly directly beneath the Scanner Pockmark. The reduced seismic velocities down to a depth of about 260 m coincide with the high amplitude, reverse polarities in the 3D seismic data that are commonly reported as evidence for free gas (Figs. 7 and 8). We observe a similar low-velocity anomaly close to the Scotia Pockmark (Fig. 7a). The seismic velocity below Scotia Pockmark is reduced down to at least 300 m. Thus, the entire anomaly beneath Scotia Pockmark may be the result of a free gas accumulation at the base of the post-glacial sediments. Due to the nature of the seismic tomography, it is quite likely that the velocity field will be smoothed and smeared out. Therefore, we attribute the mismatch between the width of the pipe structure in the 3D seismic data, i.e. 280 m, and the width of the tomography-derived velocity anomaly, i.e. 370 m, to smoothing caused by the tomographic inversion. Importantly, the velocity anomalies beneath the two pockmarks differ at depths greater than 280 m. There is a change to higher velocities underneath the Scanner Pockmark from 280 m below the surface to about 500 m. This high velocity anomaly for Scanner Pockmark is robust in the sense that almost all tomographic inversion results for different starting models show it and that the inversion result is independent of the choice of OBS ruling out picking or positioning errors. Therefore, we interpret the velocity increase to be caused by a real geological structure with different physical properties than the surrounding rocks. This interpretation matches the findings of 3D seismic attribute analysis (Böttner et al., 2019). The circular shape of the velocity anomaly (Fig. 7) supports the interpretation of this geological structure as a pipe structure. The tomographic results show that the anomaly is circular beneath the Scanner Pockmark, like other reported pipe and chimney structures (Cartwright et al., 2007; Løseth et al., 2009; Plaza-Faverola et al., 2010; Karstens and Berndt, 2015). It does not follow the shape of the tunnel valley or the distribution of free gas mapped in the 3D seismic data. A similar positive velocity anomaly may exist under Scotia Pockmark, but it is not produced by the inversion possibly because of a more limited ray coverage.

### 6.2. Nature and size of the pipe structure beneath the Scanner Pockmark

Generally, the detailed structure of pipes is poorly understood and may be variable (Cartwright et al., 2007; Gay et al., 2012). In some cases, pipe structures are associated with a positive velocity anomaly caused by diagenetic overprinting of the host rock, e.g. due to carbonate cementation within fractures (Garten et al., 2008) or gas hydrate accumulation (Plaza-Faverola et al., 2010). In other cases, the velocity anomaly is negative. Arntsen et al. (2007) proposed that such a negative velocity anomaly can be caused by a network of open fractures and ascending gas, which reduces the seismic velocities. In case of the Scanner Pockmark, the smooth 3D tomography shows up to 10% reduced seismic velocity, compared to the surrounding rocks, down to a depth of about 260 m (Figs. 8 and 9). The observation that there is no

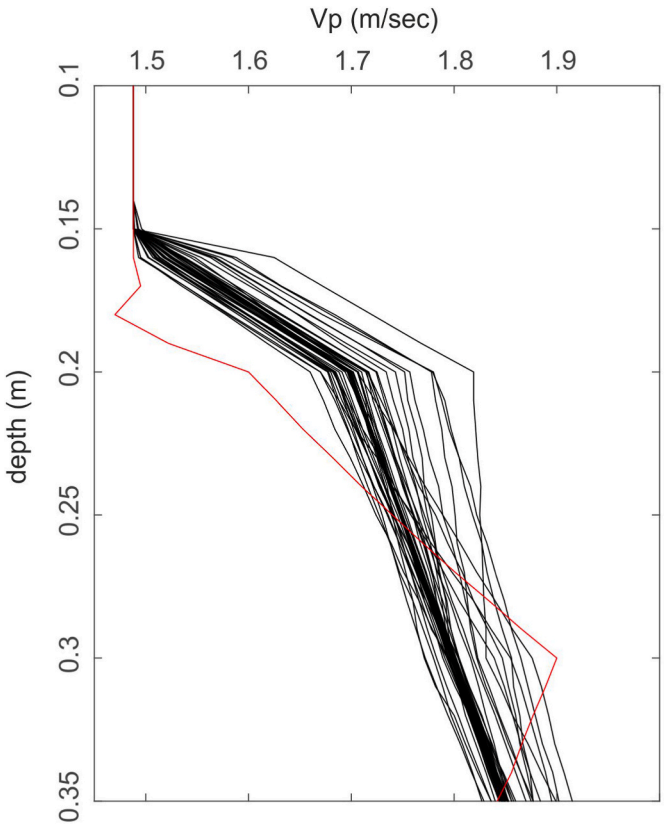


**Fig. 9.** Velocity distribution. The lines show Vp against depth. Each line corresponds to one point every 1 km across the model. The red line highlights the seismic velocity in the centre of the model, where the Scanner Pockmark is located. (For interpretation of the references to colour in this figure legend, the reader is referred to the Web version of this article.)

consistent low velocity anomaly at greater depth suggests that the gas that seeps at the seafloor originates from the accumulation of biogenic methane at the base of the glacial sediments about 50–110 m below the seafloor. Especially, with the observed seepage of gas from the seafloor (Judd et al., 1994) there is little doubt that the high amplitude, reversed-polarity reflections and the low seismic velocities are the result of free gas. It is possible that the gas is hosted in fracture networks that would further reduce the seismic velocity, but the resolution of our tomography does not allow to quantify the amount of free gas within the pipe structure. The tomographic inversion not only smooths the velocity field spatially but it also smooths the absolute velocity values. Therefore, it is likely that the seismic velocity within parts of the pipe is even more reduced or increased than 10%. The diameter of the pipe-related velocity anomaly in the inversion model is up to 370 m wide, i.e. almost twice as wide than the Scanner Pockmark. As discussed above the broad width may be due to smearing as strong differences of the velocity are smoothed during the inversion. On the other hand, characteristic tests of various possible pipe geometries show that imaging of smaller and shorter pipes is limited by the vertical resolution of the tomography. From this we conclude that the pipe structure must have at least the size of the Scanner Pockmark as smaller structures could not be resolved using our experiment setup (Fig. 1). Thus, the tomographic modelling is broadly consistent with the interpretation of the 3D seismic data that resulted in a pipe diameter of approximately 280 m (Böttner et al., 2019). The MCS data show bright spots in depths of 0.28 s and 0.35 s TWT, which correspond to glacial sediments deposited during Mid-Pleistocene (Reinardy et al., 2017). Assuming that the 3D seismic data-derived width of the pipe structure is correct, the larger pipe width in the tomographic model than in the 3D seismic data suggests that the true seismic velocity within the pipe may be as low as 150 m/s lower than the surroundings, assuming that the velocity anomaly scales with the width of the pipe.

The interpretation of the deeper part of the pipe structure is more ambiguous. The high-velocity anomaly at the centre of the pipe structure is surrounded by several-hundred-meter wide zones of decreased seismic velocities. Using characteristic tests (Fig. 6), we can rule out that this observation is caused by topographic effects related to the pronounced seafloor depressions. There is an uncertainty in the lateral extent of the pipe from MCS data and the resolution of the tomography decreases with depth. As a consequence, it is unclear whether the observed velocity anomaly (fast in the centre and slow in the surrounding area) is primarily caused by geological processes leading to an increase of seismic velocity in the centre of the pipe or processes causing a velocity decrease at the edges or the surrounding of the structure. It may be possible that the velocity decrease is a result of gas filled fractures (similar to the upper part of the pipe), which have formed by ascending fluids as the result of clogging of the pipe itself. However, it appears more likely that the low velocity zones represent the undisturbed sediments outside the pipe and the seismic anomaly is the result of increased seismic velocity inside the pipe structure. At Nyegga, gas hydrates cause an increase of seismic velocities within the local pipe structures (Plaza-Faverola et al., 2010). However, the Scanner Pockmark area is outside the gas hydrate stability zone. Alternatively, it is possible that the velocity increases because of calcite cements in the fracture network. This process has been observed in boreholes (Garten et al., 2008) and in onshore outcrops (Nielsen and Hanken, 2002). It is also possible that the pipe provides a pathway for methane to escape from the sediments, thus increasing the average velocity. In both cases, this would suggest that a fracture network in the pipe structure is not open at present. Nevertheless, even closed fracture networks that open and close episodically may still pose a lower resistance to fluid migration than the surrounding rocks that have not been affected by fluid migration. Although geophysical inversion method commonly result in an overshoot around an anomaly with the opposite sign to the core of the anomaly, the checkerboard tests and the characteristic tests do not show an overshoot (Figs. 5 and 6) suggesting that these anomalies are real and not an artefact due to the FAST algorithm. However, a final explanation for high velocities in the lower parts of the pipe can probably only be derived from drilling this part of the structure.

## 7. Conclusion

From the results of our high-resolution seismic experiment, we conclude that the pipe structure observed in seismic reflection data beneath the Scanner Pockmark is a real geological feature.

The low velocity anomaly in the upper part of the pipe corroborates the presence of free gas and we propose that it is hosted in a network of open fractures in the upper part of the pipe structure.

The nature of the deeper part of the pipe structure is less clear. The trend towards increased seismic velocities in the deep part of the pipe structure may be the result of calcite precipitation or an overprinting of the original sediment texture by fluid migration.

Overall, our study shows that a single pipe structure can be characterized by both positive and negative seismic velocity anomalies at different depths. This strongly suggests different physical properties at different depths along the pipe structure without further complications such as the presence or absence of gas hydrate accumulations (Plaza-Faverola et al., 2010). The hydraulic properties of the pipe structure are likely different than the properties of the surrounding sediments that have not been affected by fluid migration. This may be of relevance for the large-scale implementation of the geological storage of $CO_2$ in the North Sea Basin. Therefore, we suggest that a detailed, multi-method assessment of specific fluid conduits should be an essential part of $CO_2$ storage site selection.

With the available seismic data it is not possible to directly derive the hydraulic permeability of pipe structures. The lesson that the evaluation of the OBS data was severely hampered by seafloor multiples, a surface ghost, and the dimming of reflectors due to gas suggests that future geophysical investigations of pipe structures should also involve detailed tomographic inversion of surface-towed 3D seismic data with long offset streamers. This may get around the multiple and ghost problems and can make use of deeper reflections to generate velocity fields with higher resolution. Also, tomographic inversion of P-to-S converted wave arrivals may provide further insights as it would not be affected by the dimming effect of free gas and because it would provide information on the shear strength of the rocks insight the pipe structure which may reveal further indications for fracturing. Regardless, a thorough assessment of pipe structure permeability in the Central North Sea will require dedicated drilling campaigns that penetrate deeper than the base of the glacial and postglacial deposits.

## Data availability

Access to 2D seismic and OBS seismic data through Pangaea data repository (https://doi.org/10.1029/2018GC008068/https://doi.pangaea.de/10.1594/PANGAEA.915,968/https://doi.pangaea.de/10.1594/PANGAEA.932,200).

Access to 3D seismic data through PGS data library (https://www.pgs.com/data-library/europe/nw-europe/north-sea/cns). Access to Bathymetry data through EMODnet Digital Bathymetry (DTM; http://doi.org/10.12770/c7b53704-999d-4721-b1a3-04ec60c87238).

## Declaration of competing interest

The authors declare that they have no known competing financial interests or personal relationships that could have appeared to influence the work reported in this paper.

## Acknowledgements

We thank the masters and the crews of R/V Maria S. Merian cruise MSM63 and RRS James Cook cruise JC152. We thank an anonymous

reviewer and the editor for their comments helping to improve the manuscript. We thank Gaye Bayrakci, Jonathan M. Bull, Timothy J. Henstock and Tim Minshull for the support during the process of writing this manuscript. We thank PGS, Oslo for access to the MegaSurveyPlus 3D seismic data set. Access to 3D seismic data through PGS data library. (https://www.pgs.com/data-library/europe/nw-europe/north-sea/cns). We are grateful to IHS Markit for providing the KingdomSuite interpretation software within the academic licensing program. We thank the EMODnet Bathymetry Consortium (2016) for access to the EMODnet Digital Bathymetry (DTM; http://doi.org/10.12770/c7b53704-999d-4721-b1a3-04ec60c87238). This research is part of the STEMM-CCS project, which has received funding from the European Union's Horizon 2020 research and innovation program under grant agreement 654462. Additional funding for JC152 was provided by NERC grant NE/N016130/1.

## References

Andresen, K.J., 2012. Fluid flow features in hydrocarbon plumbing systems: what do they tell us about the basin evolution? Mar. Geol. 332, 89–108.
Andrews, I.J., Long, D., Richards, P.C., Thomson, A.R., Brown, S., Chesher, J.A., McCormac, M., 1990. The Geology of the Moray Firth, vol. 3. HMSO.
Arntsen, B., Wensaas, L., Løseth, H., Hermanrud, C., 2007. Seismic modeling of gas chimneys. Geophysics 72 (5), SM251–SM259.
Böttner, C., Berndt, C., Reinardy, B.T.I., Geersen, J., Karstens, J., Bull, J.M., Callow, B.J., Lichtschlag, A., Schmidt, M., Elger, J., Schramm, B., Haeckel, M., 2019. Pockmarks in the Witch Ground basin, central north sea. G-cubed 20 (4), 1698–1719.
Cartwright, J., 2007. The impact of 3D seismic data on the understanding of compaction, fluid flow and diagenesis in sedimentary basins. J. Geol. Soc. 164 (5), 881–893. https://doi.org/10.1144/0016-76492006-143.
Cartwright, J., Santamaria, C., 2015. Seismic characteristics of fluid escape pipes in sedimentary basins: implications for pipe genesis. Mar. Petrol. Geol. 65, 126–140. https://doi.org/10.1016/j.marpetgeo.2015.03.023.
Cathles, L.M., Su, Z., Chen, D., 2010. The physics of gas chimney and pockmark formation, with implications for assessment of seafloor hazards and gas sequestration. Mar. Petrol. Geol. 27, 82–91.
Chand, S., Crémière, A., Lepland, A., Thorsnes, T., Brunstad, H., Stoddart, D., 2017. Long-term fluid expulsion revealed by carbonate crusts and pockmarks connected to subsurface gas anomalies and palaeo-channels in the central North Sea. Geo Mar. Lett. 37 (3), 215–227.
Clayton, C.J., Hay, S.J., 1994. Gas migration mechanisms from accumulation to surface. Bull. Geol. Soc. Den. 41, 12–23.
Gafeira, J., Long, D., 2015. Geological Investigation of Pockmarks in the Scanner Pockmark SCI Area. JNCC Report, 570.
Garten, P., Houbiers, M., Planke, S., Svensen, H., 2008. Vent Complex at Heidrun, vol. 2008. SEG Technical Program Expanded Abstracts, pp. 809–813. https://doi.org/10.1190/1.3063767.
Gay, A., Mourgues, R., Berndt, C., Bureau, D., Planke, S., Laurent, D., Gautier, S., Lauer, C., Loggia, D., 2012. Anatomy of a fluid pipe in the Norway Basin: initiation, propagation and 3D shape. Mar. Geol. 332–334, 75–88.
Glennie, K.W., 1998. Petroleum geology of the north sea: basic concepts and recent advances. https://doi.org/10.1002/9781444313413. Fouth Edition.
Graham, A.G., Lonergan, L., Stoker, M.S., 2010. Depositional environments and chronology of Late Weichselian glaciation and deglaciation in the central North Sea. Boreas 39 (3), 471–491.
Granli, J.R., Arntsen, B., Sollid, A., Hilde, E., 1999. Imaging through gas-filled sediments using marine shear-wave data. Geophysics 64 (3), 659–992.
Haslinger, F., Kissling, E., Ansorge, J., Hatzfeld, D., Papadimitriou, E., Karakostas, V., Makropoulos, K., Kahle, G., Peter, Y., 1999. 3-D crustal structure from local earthquake tomography around the Golf of Arta (Ionian-region, NW Greece). Tectonophysics 304, 201–218.
Haszeldine, R.S., 2009. Carbon capture and storage: how green can black Be? Science 325 (5948), 1647–1652, 25 Sep. 2009.
Hovland, M., Sommerville, J.H., 1985. Characteristics of two natural gas seepages in the North Sea. Mar. Petrol. Geol. 2 (4), 319–326.
Hovland, M., Heggland, R., De Vries, M.H., Tjelta, T.I., 2010. Unit-pockmarks and their potential significance for predicting fluid flow. Mar. Petrol. Geol. 27 (6), 1190–1199.
Hubbert, M.K., Willis, D.G., 1957. Mechanic of hydraulic fracturing. Transactions of Society of Petroleum Engineers of AIME 210 (1957), 153–168.
Husen, S., Kissling, E., Flueh, E., 2000. Local earthquake tomography of shallow subduction in north Chile: a combined onshore and offshore study. J. Geophys. Res. 155, 11–32.
IPCC, 2018. Summary for policymakers. In: Masson-Delmotte, V., Zhai, P., Pörtner, H.-O., Roberts, D., Skea, J., Shukla, P.R. (Eds.), Global Warming of 1.5°C: an IPCC Special Report on the Impacts of Global Warming of 1.5°C above Pre-industrial Levels and Related Global Greenhouse Gas Emission Pathways, in the Context of Strengthening the Global Response to the Threat of Climate Change, Sustainable Development, and Efforts to Eradicate Poverty. Intergovernmental Panel on Climate Change, Geneva.
Judd, A.G., Long, D., Sankey, M., 1994. Pockmark formation and activity, UK block 15/25, North Sea. Bull. Geol. Soc. Den. 41 (1), 34–49.
Karstens, J., Berndt, C., 2015. Seismic chimneys in the Southern Viking Graben–Implications for palaeo fluid migration and overpressure evolution. Earth Planet Sci. Lett. 412, 88–100.
Karstens, J., Müller, P., Berndt, C., Patruno, S., 2019. Deep-seated focused fluid migration as indicator for hydrocarbon leads in the East Shetland Platform. North Sea Province. http://sp.lyellcollection.org/.
Kristensen, T.B., Huuse, M., 2012. Multistage erosion and infill of buried Pleistocene tunnel valleys and associated seismic velocity effects. Geol. Soc. Spec. Publ. 368, 159–172. https://doi.org/10.1144/SP368.15.
Leveque, J., Rivera, L., Wittlinger, G., 1993. On the use of the checker-board test to assess the resolution of tomographic inversions. Geophys. J. Int. 115 (1), 313–318. October 1993.
Løseth, H., Gading, M., Wensaas, L., 2009. Hydrocarbon leakage interpreted on seismic data. Mar. Petrol. Geol. 26 (7), 1304–1319.
Løseth, H., Wensaas, L., Arntsen, B., Hanken, N.-M., Basire, C., Graue, K., 2011. 1000-m long gas blow-out pipes. Mar. Petrol. Geol. 28 (5), 1047–1060.
Moss, J.L., Cartwright, J.A., 2010. The spatial and temporal distribution of pipe formation, offshore Namibia. Mar. Petrol. Geol. 27 (6), 1216–1234. https://doi.org/10.1016/j.marpetgeo.2009.12.013.
Nielsen, J.K., Hanken, N., 2002. Late Permian carbonate concentration in the marine siliciclastic sediments of the Ravnefjeld Formarion, East Greenland. Geology of Greenland Survey Bulletin 191, 126–132.
Plaza-Faverola, A., Westbrook, G.K., Ker, S., Exley, R.J.K., Gailer, A., Minshull, T.A., Broto, K., 2010. Evidence from three-dimensional seismic tomography for a substantial accumulation of gas hydrate in a fluid-escape chimney in the Nyegga pockmark field, offshore Norway. J. Geophys. Res.: Solid Earth 115. Issue B8.
Rea, B.R., Newton, A.M., Lamb, R.M., Harding, R., Bigg, G.R., Rose, P., Buckley, F., 2018. Extensive marine-terminating ice sheets in Europe from 2.5 million years ago. Science advances 4 (6), eaar8327.
Reinardy, B.T., Hjelstuen, B.O., Sejrup, H.P., Augedal, H., Jørstad, A., 2017. Late Pliocene-Pleistocene environments and glacial history of the northern North Sea. Quat. Sci. Rev. 158, 107–126.
Schmelzbach, C., Zelt, C.A., Juhlin, C., Carbonell, R., 2008. P- and SV-velocity structure of the South Portuguese Zone fold-and-thrust belt, SW Iberia, from traveltime tomography. Geophys. J. Int. 175 (2), 689–712. November 2008.
Schneider von Deimling, J., Brockhoff, J., Greinert, J., 2007. Flare imaging with multibeam systems: data processing for bubble detection at seeps. G-cubed 8 (6).
Sejrup, H.P., Aarseth, I., Ellingsen, K.L., Reither, E., Jansen, E., Løvlie, R., Stoker, M., 1987. Quaternary stratigraphy of the Fladen area, central North Sea: a multidisciplinary study. J. Quat. Sci. 2 (1), 35–58.
Stoker, M.S., Balson, P.S., Long, D., Tappin, D.R., 2011. An Overview of the Lithostratigraphical Framework for the Quaternary Deposits on the United Kingdom Continental Shelf.
Yu, Y., Kelley, C.L., Mardanova, I.M., 2015. U.S. Patent No. 9,105,075. U.S. patent and Trademark Office, Washington, DC.
Zelt, C.A., 1998. Lateral velocity resolution from three-dimensional seismic refraction data. Geophysical Journal of Geophysical Research 135, 1101–1112.
Zelt, C.A., Barton, P.J., 1998. Three-dimensional seismic refraction tomography: a comparison of two methods applied to data from the Faeroe Basin. J. Geophys. Res.: Solid EarthVolume 103. Issue B4.